Composite Structures 280 (2022) 114757

Contents lists available at ScienceDirect

Composite Structures

journal homepage: www.elsevier.com/locate/compstruct

Multi-objective optimisation designs for thin-walled deployable composite hinges using surrogate models and Genetic Algorithms

Tian-Wei Liu [a], Jiang-Bo Bai [a,b,*], Nicholas Fantuzzi [c], Guang-Yu Bu [a], Dong Li [a]

[a] School of Transportation Science and Engineering, Beihang University, Beijing 100191, PR China
[b] Jingdezhen Research Institute of Beihang University, Jiangxi Province 333000, PR China
[c] DICAM Department, University of Bologna, Bologna 40136, Italy

ARTICLE INFO

Keywords:
Deployable composite hinge (DCH)
Multi-objective optimisation
Surrogate models
Genetic Algorithms
Benchmarking

ABSTRACT

Thin-walled deployable composite hinges (DCHs) can achieve foldable and deployable functions by storing and releasing strain energy, which have great application potential in deployable structures, such as satellite antennas and solar wings. This paper presented multi-objective optimisation designs for DCHs. Firstly, an optimisation problem was established to obtain three conflicting objectives, minimising the peak folding moment, maximising the peak torsional moment and minimising the mass. Three design variables and one constraint had been considered. Moreover, four surrogate models were employed, including response surface methodology (RSM) and machine learning models. Root mean square error (RMSE), mean absolute error (MAE) and correlation coefficient (R^2) were used to determine the surrogate model with the highest accuracy. Furthermore, four state-of-the-art Genetic Algorithms were benchmarked to obtain the optimal designs. The mimicked inverted generational distance (mIGD) was applied to determine the best optimiser. The research results have significance to practical engineering application of DCHs.

1. Introduction

Due to the limitation of launch vehicles, there are many structures with folding and deployable mechanism on the spacecraft, such as synthetic aperture radars (SARs), solar arrays and booms, etc. These structures must be packed into compact volume for launching and also be able to deploy in the operational state [1–3]. Previous solutions used rigid rod assemblies with mechanical hinges which were usually driven by electric motors. Although these designs can satisfy simultaneously multiple requirements for stiffness, stability and deployment repeatability, mechanical hinges and electric motors increase weight of the spacecraft. For substiting traditional mechanical deployable structures, light weight deployable composite structures have attracted widespread attention [4–10]. The circular composite tube with symmetrical slots on both sides is one of the classical deployable composite hinges (DCHs). Tubular DCHs have an integral hinge mechanism which can realize the foldable and deployable functions, as shown in Fig. 1. It can take advantage of the elastic strain energy stored during folding to realize automatic deployment without electric motor driving; after deployment, it also can provide the locking force required by the deployable structure through its own stiffness without additional locking device. DCHs have several advantages over traditional mechanical hinges, including lightweight, self-deployment, self-locking and good latching accuracy, etc [11–15]. Therefore, DCHs have good engineering application prospects, and it is necessary to optimise them to obtain the optimal designs.

Coupling surrogate model (SM) and Genetic Algorithm (GA) technology, as a hybrid optimisation method, has been widely employed in many fields of engineering [16–24]. In this technology, a SM which can determine the relationship between design variables and objectives is firstly obtained, and then the SM and a GA are coupled to obtain the optimal design solutions. SMs, also called metamodeling, mainly include the response surface methodology (RSM) model and machine learning models. The RSM model is a widely used statistical tool that is able to find the relationship between design variables and objectives through statistical fitting method to establish predictive equations, in which numerous design variables and their collaborations jointly affect the response results [25]. The most widely used RSM model is the Box-Behnken which provides considerable fitting accuracy for most problems. However, the RSM exhibits weak performance in describing highly nonlinear problems, which can be solved by applying machine learning models. In recent years, machine learning models have become an important tool for accurately modeling higher-order and nonlinear problems. The key concept of machine learning models is to learn useful

* Corresponding author at: School of Transportation Science and Engineering, Beihang University, Beijing 100191, PR China.
E-mail address: baijiangbo@buaa.edu.cn (J.-B. Bai).

https://doi.org/10.1016/j.compstruct.2021.114757
Received 5 July 2021; Accepted 24 September 2021
Available online 30 October 2021

Nomenclature

$d(\nu, O)$	the minimum Euclidean distance between ν and the points in O
D	end-section diameter, mm
E_1	elastic modulus of composite ply in longitudinal direction, GPa
E_2	elastic modulus of composite ply in transverse direction, GPa
G_{12}	in-plane shear modulus of composite ply, GPa
l	slot length, mm
L	total length, mm
m	mass, g
M_1	peak folding moment, N·mm
M_2	peak torsional moment, N·mm
M^*	a set of points along the mimicked Pareto front
N	number of FEA values
P	number of input variables
S_{12}	in-plane shear strength of composite ply, MPa
t	thickness of total composite plies, mm
w	slot width, mm
x	input data
x_{norm}	normalised of input data
$x_{\min}$	minimum of input data
$x_{\max}$	maximum of input data
X_{1t}	tensile strength of composite ply in longitudinal direction, MPa
X_{2c}	compressive strength of composite ply in longitudinal direction, MPa
Y_{1t}	tensile strength of composite ply in transverse direction, MPa
Y_{2c}	compressive strength of composite ply in transverse direction, MPa
Y	predicted value
$Y_{i,\text{FEA}}$	i^{th} FEA value
$Y_{i,\text{pre}}$	i^{th} predicted value by surrogate model
Y_{FEA}	average value of all FEA values
O	a set of points from the currently obtained Pareto front
α	torsional failure angle, deg
β_0	regression coefficient
β_i	coefficient
β_{ii}	coefficient
β_{ij}	coefficient
β_{iii}	coefficient
β_{iij}	coefficient
ρ	density of composite, g/cm^3
χ^2	chi square statistics
ν_{12}	poisson's ratio
ANOVA	analysis of variance
AP	accuracy prediction
APD	angle penalized distance
ANN	artificial neural network
C	cost of constraint violation
CEC'09	IEEE congress on evolutionary computation 2009
CV	coefficient of variation
d1	Willmott's index of agreement
DCH	deployable composite hinge
DF	degree of freedom
DTLZ	Deb-Thiele-Laumanns-Zitzler
FEA	finite element analysis
GA	Genetic Algorithm
GD	generational distance
HV	hyper volume
IDG	inverted general distance
mIGD	mimicked inverted general distance
min_samples_split	the minimum number of samples required to split internal nodes
max_depths	the maximum depth of regression trees
MOEA/D	multi-objective evolutionary algorithm based on decomposition
MOEA/DD	multi-objective evolutionary algorithm based on dominance and decomposition
MTS	multiple trajectory search
MAE	mean absolute error
MSE	mean square error
MS	maximum spread
MPE	mean predictive error
n_estimators	the number of regression trees
ε-svr	epsilon regression
nu-svr	nu regression
eps-svr	bound-constraint regression
R^2	correlation coefficient
Adj-R^2	adjusted correlation coefficient
Pred-R^2	predicted correlation coefficient
ReLU	Rectified Linear Unit
HYBRID	hybrid fractional error function
NSGA-II	nondominated sorting genetic algorithm II
NSGA-III	non-dominated sorting genetic algorithm III
SPEA-II	strength pareto evolutionary algorithm II
SAR	synthetic aperture radar
SM	surrogate model
SVM	support vector machine
SVR	support vector regression
SS	sum of square
RBF	radial basis function
RF	random forest
RMSE	root mean square error
RMS	response surface methodology
RVEA	reference vector guided evolutionary algorithm

patterns from previous dataset and to generate rigorous models by means of mapping data [26].

GAs are one of the most popular categories of optimisation techniques, especially in engineering design, because they can find optimal designs in a large and complex search space [27]. Multi-objective optimisation designs can be solved by two methods, namely the weighted average method and the Pareto front solution. The weighted average method reduces multiple objectives to a single objective by utilising Weighted Sum Method, which requires prior knowledge of the relative importance of all objectives. However, the traditional weighted average method cannot solve multi-objective optimisation designs effectively. Therefore, the Pareto front solution is generally considered to be the most interesting category. Designers can obtain a better understanding of the domain according to the Pareto front, from which they can select design solutions that match other considerations not included in the optimisation design [28]. A recent literature [29] exhibits that representative GAs based on dominance strategy and decomposition strategy are suitable for different optimisation problems. Therefore, in order to better balance the convergence and diversity of multi-objective optimisation problems, especially many-objective (4–15 objectives), some novel hybrid multi-objective GAs have been proposed, which combine dominance strategy with decomposition strategy.

In summary, it can be concluded that DCHs have many advantages over traditional mechanical hinges. However, few scholars employed

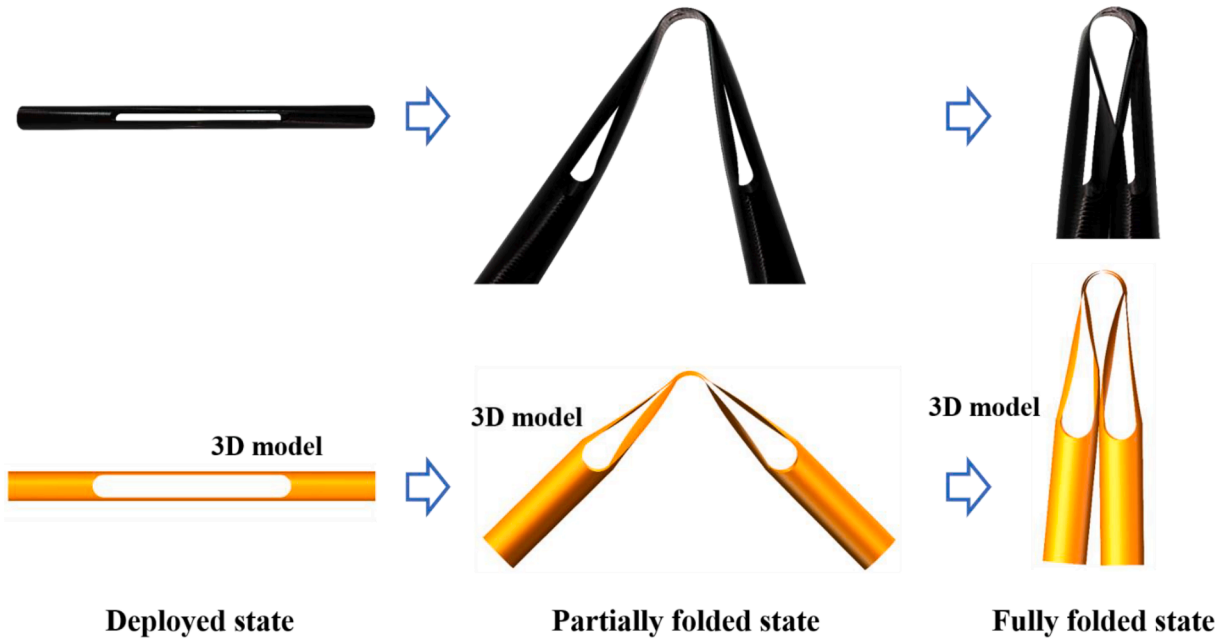

Fig. 1. Folding deformation process of the tubular DCH.

coupling SM and GA technology to obtain the optimal designs of DCHs (such as the maximum peak torsional moment, the minimum peak folding moment and the minimum mass). In this paper, based on the dataset of folding and torsional behaviours of DCHs calculated from finite element analysis (FEA) method, four SMs were obtained to determine the relationship between the design variables and the objectives. These four SMs employed for the benchmarking include: Box-Behnken design of the RSM model and three most popular machine learning models, namely artificial neural networks (ANN), support vector regression (SVR) and random forest (RF). The four SMs were ranked according to the prediction accuracy by three statistical error functions: root mean square error (RMSE), mean absolute error (MAE) and correlation coefficient (R^2). Then, based on the SM with the highest prediction accuracy and the analytical formula of mass, four state-of-the-art GAs were benchmarked to solve the multi-objective optimisation designs of the peak folding moment, the peak torsional moment and the mass of DCHs. The optimal design solutions of DCHs were found. The GAs employed for benchmarking include: strength pareto evolutionary algorithm II (SPEA-II) which generally performs well on all problem sets, and three popular hybrid GAs, namely non-dominated sorting genetic algorithm III (NSGA-III), multi-objective evolutionary algorithm based on dominance and decomposition (MOEA/DD) and reference vector guided evolutionary algorithm (RVEA). Each GA was independently run 30 cycles to eliminate the effect of the randomness of the initial population. The best performing optimiser was quantitatively determined by applying mimicked inverted general distance (mIGD).

The paper is organised as follows: the formulation and the methodology of the multi-objective optimisation designs are detailed in Section 2; the benchmarking results of the four SMs are summarised in Section 3; the benchmarking results of the four state-of-the-art GAs are discussed in Section 4; the optimal design solutions are analysed in Section 5; three key findings are summarised in Section 6.

2. Optimal design methods of tubular deployable composite hinges

2.1. Problem description

In the folding process of DCHs, the peak folding moment should be as small as possible to avoid excessive impact. In working state, DCHs may

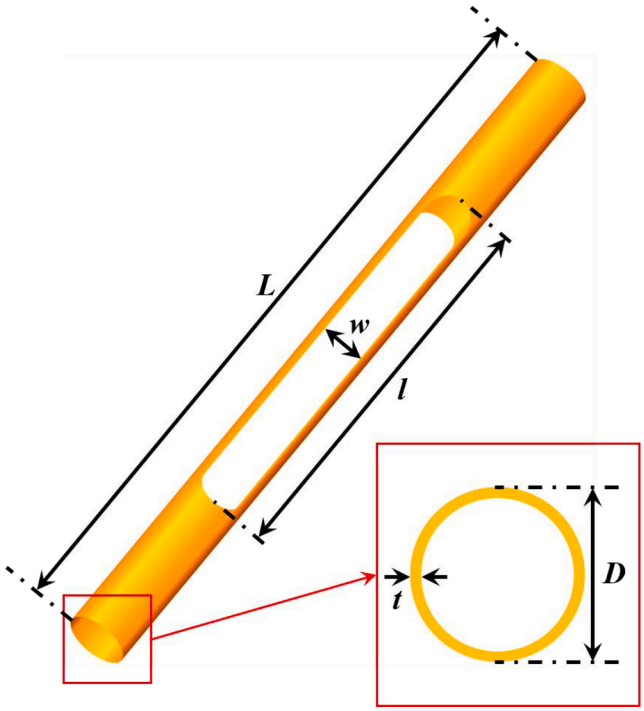

Fig. 2. Geometric model of the tubular DCH.

be subjected to torsional excitation. Therefore, DCHs need to have enough peak torsional moment to resist external torsion excitation. In addition, the mass of DCHs should be as small as possible to reduce the cost of its application in space missions. In summary, the maximum peak torsional moment, the minimum peak folding moment and the minimum mass were set as the optimisation objectives of DCHs. In order to resist the possible torsional deformation of DCHs in working state, the torsional failure angle was set as a constraint.

Many investigations showed that geometric parameters of DCHs have significant effects on folding behaviour, torsional behaviour and mass. Therefore, three geometric parameters were taken into

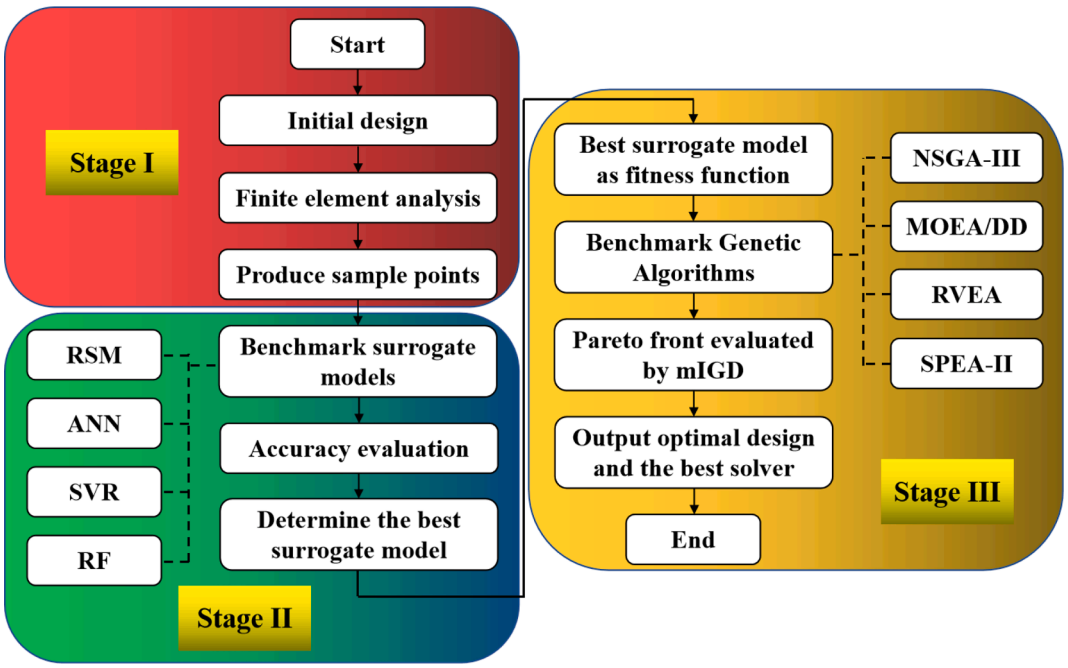

Fig. 3. Optimal program flowchart of DCHs.

consideration as design variables, as follows (shown in Fig. 2):

- the end-section diameter, D;
- the slot width, w;
- the slot length, l.

The multi-objective optimisation problem of DCHs was formulated in a constrained format in Eq. (1) as,

$$\begin{cases} \min \mathrm{M}_1(\mathrm{D},\ \mathrm{w},\ \mathrm{l}),\ \mathrm{m}(\mathrm{D},\ \mathrm{w},\ \mathrm{l}) \\ \quad maxM_2(D,\ w,\ l) \\ \quad \text{subjectto}: \\ \mathrm{g}(D,\ w,\ l) = \alpha - \alpha_{min} > 0, \\ \quad \underline{x_i} \leqslant x_i \leqslant \overline{x}_i (i = 1, 2, 3), \end{cases} \tag{1}$$

where $\boldsymbol{x} = [x_1,\ x_2,\ x_3]$ are the design variables, $M_1(D,\ w,\ l)$ and $M_2(D,\ w,\ l)$ are respectively the peak folding moment and the peak torsional moment of DCHs, m is the mass of DCHs, $\mathrm{g}(D,\ w,\ l) > 0$ is the constraint of the torsional failure angle of DCHs, α and α_{min} are the torsional failure angle and the minimum torsional failure angle, respectively, and $\underline{x_i}$ and $\overline{x_i}$ are the upper and lower limits of the domain, respectively.

The mass of a DCH is expressed in Eq. (2) as,

$$m = t\rho D\left(\pi L - 2larcsin\frac{w}{D} - \frac{1}{2}\pi warcsin\frac{w}{D}\right), \tag{2}$$

where ρ is the density of composite.

Penalty techniques are general methods to solve constraints in optimisation problems. However, penalty techniques require user-defined problem-dependent parameters, which usually have a negative effect on the performance of the GAs. Adaptive penalty techniques automatically set the values of all involved parameters using the feedback from the search process without user intervention. Therefore, adaptive penalty techniques [30–32] have been attracted widespread attention. An adaptive penalty technique for dealing with the constraints in optimisation problems was applied in this paper. A penalty coefficient was set in the fitness function. For any feasible solution, the penalisation coefficient was 1; for any unfeasible solution, the penalisation coefficient was greater than 1. Furthermore, the penalisation coefficient was increased with the increased magnitude of the constraint violation. The reader refers to Barbosa et al. [32] for a detailed introduction to the adaptive penalty technique.

Table 1
Design space of the optimisation problem.

Design variable	Type	Lower bound	Upper Bound
D (mm)	continuous	55	65
w (mm)	continuous	30	50
l (mm)	continuous	150	210

2.2. Methodology

The multi-objective optimisation model of DCHs was obtained by using coupling SM and GA technology. The detailed modeling process is as follows (shown in Fig. 3):

(1) Stage I: The FEA method was utilised to obtain the dataset required by the SMs. The dataset used in this study is taken from the literature [15]. Su et al. [15] used ABAQUS/Explicit solver to simulate the folding and torsion processes of DCHs, in which four-node reduced integrated shell elements (S4R) were employed. The Hashin failure criterion was selected to determine the damage of DCHs during the folding and torsion deformation process. The domain and the type of each design variable of the optimisation problem are summarised in Table 1. The minimum torsional failure angle was set to 10°. In order to achieve a comprehensive Pareto front and evaluate the performance of each benchmarked GA, the design variables were set as continuous variables. The specifications and properties of DCHs and 79 FEA results are listed in Table A1 and A2, respectively.
(2) Stage II: the 79 FEA results were used as the dataset to establish the SMs. The SMs utilised in this research include RSM model and three machine learning models, namely ANN, SVR and RF. The prediction results of the four SMs were compared by three statistical error functions, including RMSE, MAE and R^2.
(3) Stage III: the SM with the highest prediction accuracy and the analytical formula of mass were coupled with GAs to optimise

Table 2
ANOVA analyses for the dataset of Box-Behnken design.

Source	DF	Peak folding moment			Peak torsional moment			Torsional failure angle		
		SS	*F*-value	*p*-value	SS	*F*-value	*p*-value	SS	*F*-value	*p*-value
Model	19	7.753E + 010	130.21	< 0.0001	1.669E + 010	417.23	< 0.0001	968.70	65.48	< 0.0001
A-*D*	1	5.879E + 008	18.76	< 0.0001	3.317E + 007	15.76	0.0002	19.93	25.60	< 0.0001
B-*w*	1	8.085E + 008	25.80	< 0.0001	2.582E + 007	12.27	0.0008	24.80	31.85	< 0.0001
C-*l*	1	9.454E + 007	3.02	0.0865	1.551E + 006	0.74	0.3935	0.39	0.50	0.4801
AB	1	2.957E + 009	94.36	< 0.0001	6.016E + 008	285.78	< 0.0001	423.22	543.54	< 0.0001
AC	1	1.020E + 009	32.56	< 0.0001	2.212E + 008	105.06	< 0.0001	135.87	174.49	< 0.0001
BC	1	2.377E + 009	75.85	< 0.0001	1.934E + 006	0.92	0.3410	11.58	14.87	0.0002
A^2	1	7.667E + 007	2.45	0.1220	1.270E + 008	60.32	< 0.0001	56.94	73.12	< 0.0001
B^2	1	2.710E + 009	86.48	< 0.0001	2.603E + 007	12.37	0.0007	22.86	29.35	< 0.0001
C^2	1	5.459E + 008	17.42	< 0.0001	3.019E + 007	14.34	0.0003	11.87	15.24	0.0002
ABC	1	6.093E + 007	1.94	0.167	1.097E + 008	52.12	< 0.0001	44.74	57.46	< 0.0001
A^2B	1	2.585E + 007	0.82	0.3666	7.414E + 007	35.22	< 0.0001	36.14	46.41	< 0.0001
A^2C	1	2.214E + 008	7.06	0.0096	1.067E + 007	5.07	0.0273	4.09	5.25	0.0248
AB^2	1	1.232E + 007	0.39	0.5326	2.931E + 008	139.22	< 0.0001	153.60	197.27	< 0.0001
AC^2	1	1.561E + 008	4.98	0.0286	1.066E + 006	0.51	0.4788	1.31	1.68	0.1987
B^2C	1	2.924E + 007	0.93	0.3372	7.306E + 006	3.47	0.0664	0.51	0.66	0.4203
BC^2	1	47389.50	1.512E-003	0.9691	6.875E + 006	3.27	0.0747	6.13	7.88	0.0064
A^3	1	2.751E + 007	0.88	0.3518	1.091E + 007	5.18	0.0257	1.91	2.46	0.1212
B^3	1	1.329E + 007	0.42	0.5169	3.277E + 007	15.57	0.0002	15.08	19.36	< 0.0001
C^3	1	56801.13	1.813E-003	0.9662	1.445E + 006	0.69	0.4101	0.53	0.68	0.4121
Residual	75	2.350E + 009			1.579E + 008			58.40		
Cor total	94	7.988E + 010			1.685E + 010			1027.10		
Std. Dev		5597.94			1540.91			0.88		
Mean		64634.85			27250.16			13.56		
CV%		8.66			5.32			6.51		
PRESS		3.906E + 009			2.624E + 008			97.33		
Adeq. Prec		46.54			81.09			33.54		
R^2		0.971			0.991			0.943		
Adj-R^2		0.963			0.988			0.929		
Pred-R^2		0.951			0.984			0.905		

SS = Sum of square, DF = Degree of freedom.

DCHs. Bai et al. [33] pointed out that benchmarking is necessary when the relationship between the shape of the codomains and the domain is unknown. Benchmarking process helps to understand the nature of the optimisation problem and to determine the best performance of the GA. The benchmarking results from IEEE congress on evolutionary computation 2009 (CEC'09) [34] were applied to select the optimisers for the optimisation of the peak folding moment, the peak torsional moment and the mass of DCHs. The multi-objective GAs benchmarks include: a general optimiser SPEA-II and three popular hybrid GAs, namely NSGA-III, MOEA/DD and RVEA.

For Stage II, parameter tuning for the three machine learning models is very important to obtain the desired results. In order to test the three machine learning models fairly, the grid search method was employed to tune parameters in the best way to obtain the best results. For Stage III, the SM with the highest accuracy and the analytical formula of mass were utilised to evaluate all individuals from the population. In order to perform a fair test across the four Gas, the same genetic operator types were used: selection, crossover and mutation, as well as the same operator rate those were selected for the CEC'09 benchmarking [34].

3. Determining the best surrogate model

3.1. Response surface methodology

RSM is an experimental statistical modeling technique for multiple regression analysis. RSM can determine the relationship between input and output of a complex system. Typical RSM models include: fractional factorial designs, the steepest rise stroke, Doehlert and blend designs, Box-Behnken and central composite design [35]. The most widely used Box-Behnken design (Design-Expert Software, Version 8.0.6, from Stat-Ease, Inc.) was selected in this paper to obtain the relationship between design variables and objectives. The third-order regression equation proposed according to Box-Behnken design is as follows:

$$Y = \beta_0 + \sum \beta_i x_i + \sum \beta_{ii} x_i^2 + \sum\sum \beta_{ij} x_i x_j + \sum \beta_{iii} x_i^3 + \sum\sum \beta_{iij} x_i^2 x_j + \varepsilon, \tag{3}$$

Where Y is the predicted value, β_0 is the regression constant, β_i, β_{ii}, β_{ij}, β_{iii} and β_{iij} are all coefficients, and ε is the random error.

The third-order equation with the three design variables can be obtained in Eq. (4) as,

$$\begin{aligned} Y = {} & \beta_0 + \beta_1 x_1 + \beta_2 x_2 + \beta_3 x_3 + \beta_{11} x_1^2 + \beta_{22} x_2^2 + \beta_{33} x_3^2 + \beta_{12} x_1 x_2 + \beta_{13} x_1 x_3 + \beta_{23} x_2 x_3 + \beta_{111} x_1^3 \\ & + \beta_{222} x_2^3 + \beta_{333} x_3^3 + \beta_{112} x_1^2 x_2 + \beta_{113} x_1^2 x_3 + \beta_{221} x_2^2 x_1 + \beta_{223} x_2^2 x_3 + \beta_{331} x_3^2 x_1 + \beta_{332} x_3^2 x_2 + \varepsilon. \end{aligned} \tag{4}$$

The third-order equations of three objectives (i.e. $M_1(D,\ w,\ l)$, $M_2(D,\ w,\ l)$ and $g(D,\ w,\ l)$) of DCHs optimisation are listed in Appendix B.

Analysis of variance (ANOVA) was carried out to evaluate the

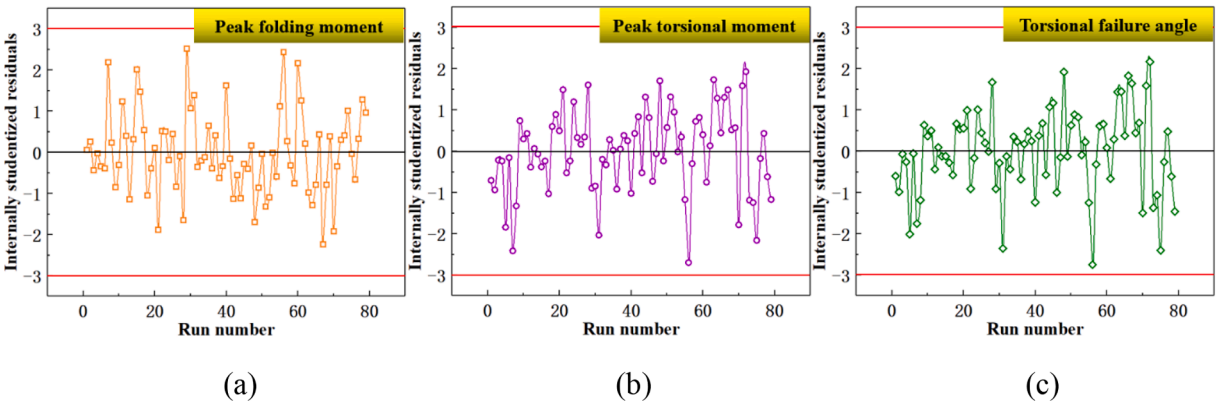

Fig. 4. Residual distribution diagram against the test steps: (a) Peak folding moment (b) Peak torsional moment (c) Torsional failure angle.

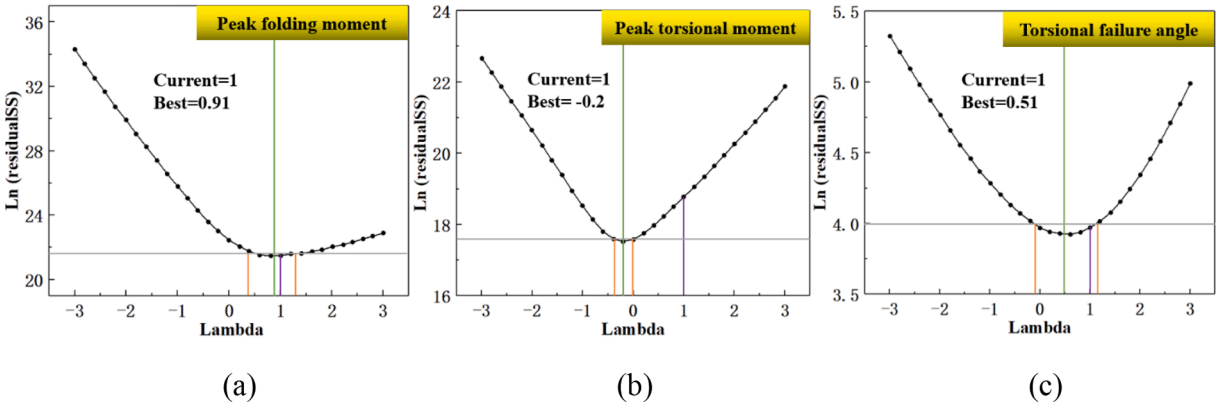

Fig. 5. Box-Cox charts: (a) Peak folding moment (b) Peak torsion moment (c) Torsional failure angle.

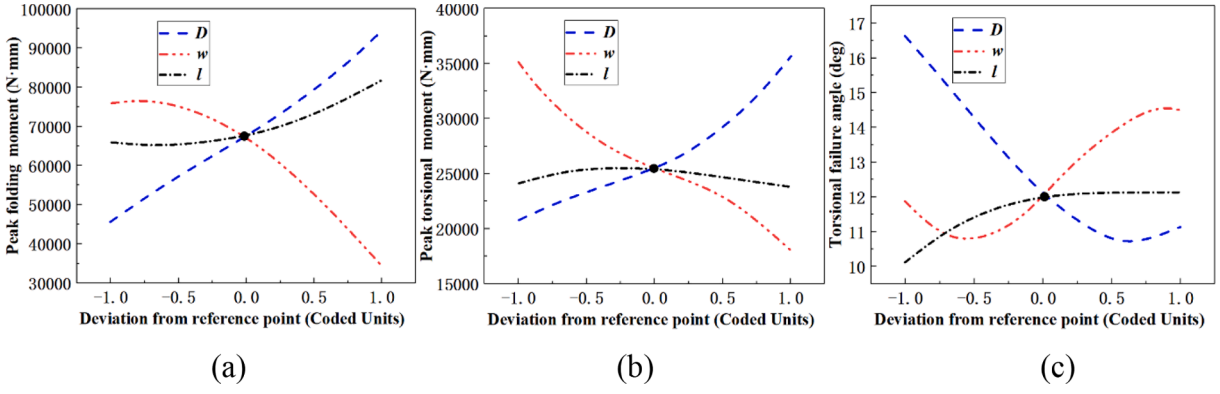

Fig. 6. Perturbation charts: (a) Peak folding moment (b) Peak torsion moment (c) Torsional failure angle.

prediction accuracy and significance of the regression models. The results show that the regression equations in Appendix B fully reflect the relationship between the design variables and the objectives. Table 2 shows the ANOVA values of the peak folding moment, the peak torsional moment and the torsional failure angle. The F-test compares the source's mean square to the residual mean square, while p value is the probability of the observed F value. These two values are applied to examine the significance of the regression models. A higher F value and a lower p value (<0.05) can prove that the regression models are significant. According to Table 2, the F value of the three regression models is higher and the p value is lower, so the significance of the three regression models can be inferred. Adequate precision (AP) parameter value above 4 indicates the regression model is effective. Because it can measure the signal to noise ratio and compare the range of the predicted value to the average prediction error. The adequate precision (AP) parameter values of the three regression models are 46.54, 81.09 and 33.54 respectively, indicating that the signal is sufficient. In addition, the coefficient of variance (CV) is the standard error ratio estimated by the mean of the response, and it shows the reproducibility of the regression model. If the CV value is not greater than 10%, it can be concluded that the regression model is reproducible. The CV values of the three regression models are respectively 8.66%, 5.32% and 6.51%, indicating that the three regression models are reproducible. The R^2 of the three regression models are 0.971, 0.991 and 0.943 respectively, which shows that the

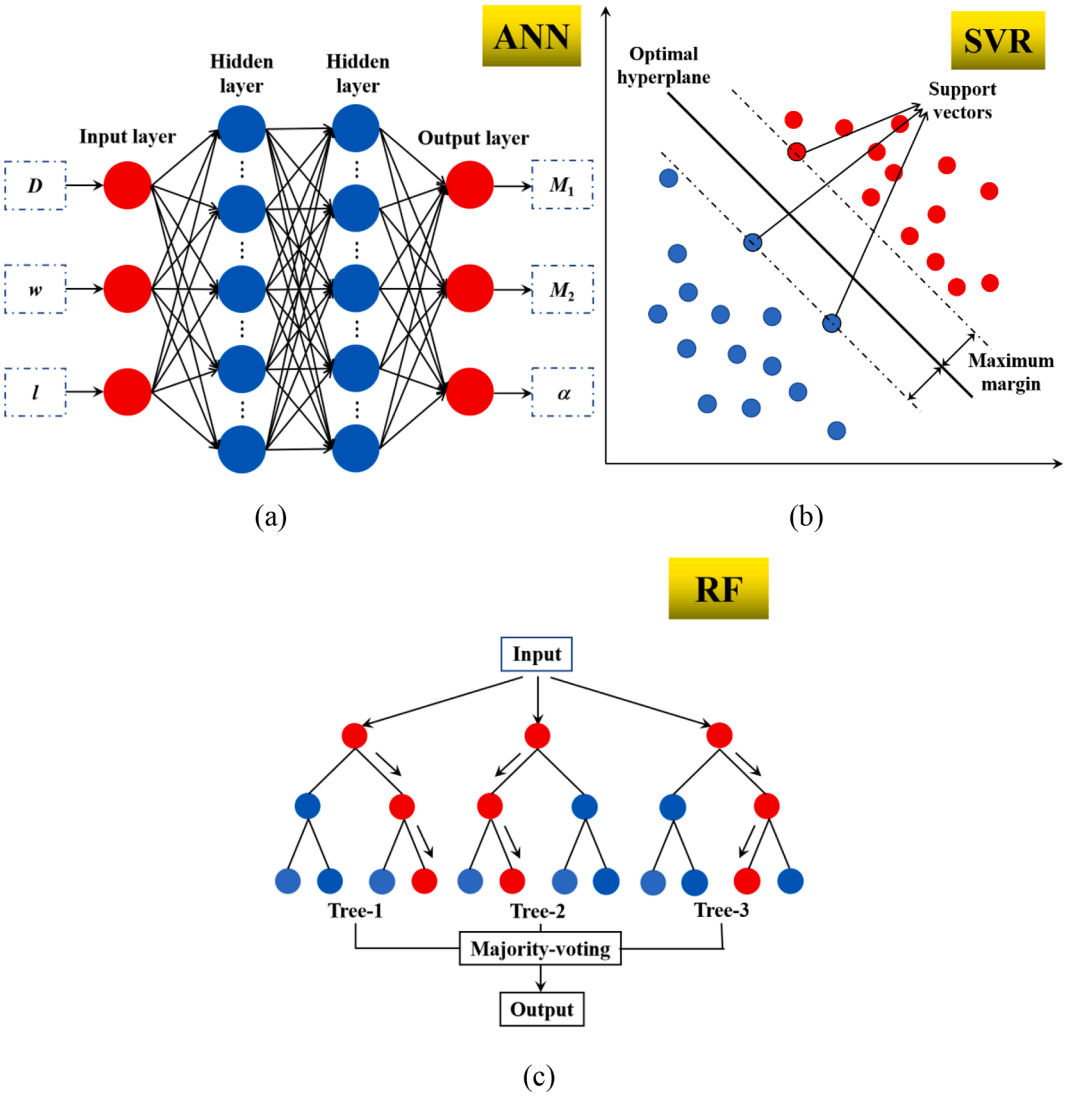

Fig. 7. Schematic diagrams of popular machine learning models: (a) ANN (b) SVR (c) RF.

predicted values are in good agreement with the FEA values. Besides, the low difference between Adj-R^2, Pred-R^2 and R^2 shows that all factors are significant and effective for the three regression models.

Fig. 4 shows the residual distribution of 79 FEA values. The results indicate that the error between the FEA values and predicted values is less than ± 3%, and the input value and output value are in good agreement with each other. Table 5 shows the Box-Cox graphs of the folding behaviour and the torsional behaviour of DCHs, which helps determine the most appropriate power transfer function to apply the response. In the Box-Cox chart, the lowest point represents the best Lambda value where the minimum sum of squares is created in the converted model (shown in Fig. 5). When the ratio of maximum to minimum response is greater than 3, it will have a greater ability to improve the model utilising power functions. The *F* value in ANOVA and perturbation plot can reflect the ability of each factor to affect the response. According to Table 2 and Fig. 6, the *F* values of the end-section diameter and the slot width of the three regression models are larger, and the three objectives change significantly with the change of the end-section and the slot width. It is indicated that the end-section diameter and the slot width have a greater influence on the three objectives. On the contrary, the slot length has little effect on the three objectives.

In summary, the third-order regression equations have high prediction accuracy for the peak folding moment, the peak torsional moment and the torsional failure angle of DCHs. In addition, the significance and effectiveness of the second-order regression equations are investigated by ANOVA. Although the second-order regression equations are also significant, they will not be discussed because of low prediction accuracy.

3.2. *Machine learning models*

As substitutes for the RSM model, machine learning models are increasingly used in engineering practice. In this paper, three most popular machine learning models (i.e. ANN, SVR and RF) were employed to predict the peak folding moment, the peak torsional moment and torsional failure angle of DCHs. The schematic diagrams of the three machine learning models are shown in Fig. 7. Handhal et al. [36] and Shozib et al. [37] introduced the detailed mechanisms of ANN, SVR and RF. In addition, parameter tuning for machine learning model is essential to obtain desired results. The grid search method was employed to tune parameters in the best way to obtain the best predicted results.

Table 3
Statistical error functions.

Error function	Equation	Number
Root mean square error [38]	$RMSE = \sqrt{\frac{1}{N}\sum_{i=1}^{N}\left(Y_{i,\mathrm{FEA}} - Y_{i,\mathrm{pre}}\right)^2}$	(6)
Mean square error [39]	$MSE = \frac{1}{N}\sum_{i=1}^{N}\left(Y_{i,\mathrm{FEA}} - Y_{i,\mathrm{pre}}\right)^2$	(7)
Mean absolute error [40]	$MAE = \frac{1}{N}\sum_{i=1}^{N}\left\lvert Y_{i,\mathrm{FEA}} - Y_{i,\mathrm{pre}}\right\rvert$	(8)
Mean predictive error (%) [41]	$MPE(\%) = \frac{100}{\mathrm{N}}\sum_{i=1}^{\mathrm{N}}\left\lvert\frac{\mathrm{Y_{i,FEA}} - \mathrm{Y_{i,pre}}}{\mathrm{Y_{i,FEA}}}\right\rvert$	(9)
Chi square statistics (χ^2) [42]	$\chi^2 = \sum_{i=1}^{N}\frac{\left(Y_{i,\mathrm{pre}} - Y_{i,\mathrm{FEA}}\right)^2}{Y_{i,\mathrm{pre}}}$	(10)
Correlation coefficient (R^2) [43]	$R^2 = 1 - \frac{\sum_{i=1}^{N}\left(Y_{i,\mathrm{pre}} - Y_{i,\mathrm{FEA}}\right)^2}{\sum_{i=1}^{N}\left(Y_{i,\mathrm{FEA}} - Y_{\mathrm{FEA}}\right)^2}$	(11)
Adjusted correlation coefficient (Adj-R^2) [44]	$\mathrm{Adj}-R^2 = 1 - \left[\frac{(1-\mathrm{R}^2)(\mathrm{N}-1)}{\mathrm{N}-\mathrm{P}-2}\right]$	(12)
Willmott's index of agreement (d1) [45]	$d1 = 1 - \frac{\sum_{i=1}^{N}\left\lvert Y_{i,\mathrm{pre}} - Y_{i,\mathrm{FEA}}\right\rvert}{\sum_{i=1}^{N}\left\lvert Y_{i,\mathrm{FEA}} - Y_e\right\rvert + \left\lvert Y_{i,\mathrm{pre}} - Y_e\right\rvert}$	(13)
Hybrid Fractional Error Function [46]	$HYBRID = \frac{100}{N-P}\sum_{i=1}^{N}\frac{\left(Y_{i,\mathrm{FEA}} - Y_{i,\mathrm{pre}}\right)^2}{Y_{i,\mathrm{FEA}}}$	(14)

Note: N is the number of FEA values, $Y_{i,\mathrm{FEA}}$ is the i^{th} FEA value, $Y_{i,\mathrm{pre}}$ is the i^{th} predicted value by SMs, Y_{FEA} is the average value of all FEA values and P is the number of input variables.

3.2.1. Data normalisation

Data normalisation is necessary for organising the dataset to reduce redundancy and improve dataset integrity. There are a lot of types of normalisation methods, such as StandardScaler, MinMaxScalar, RobustScaler and DecimalScaler. The choice of a normalisation method depends on the application and the algorithm that uses the normalised dataset. In this research, the dataset was normalised in the range [0, 1] applying MinMaxScalar function according to the Eq. (5):

$$x_{\mathrm{norm}} = \frac{x - x_{min}}{x_{max} - x_{min}}, \tag{5}$$

Where x_{norm}, x, x_{min} and x_{max} are the normalised, initial, minimum, and maximum of input data, respectively.

3.2.2. Artificial neural network

ANN is an information processing system based on mimicking the structure and function of biological neural systems of human brain, and it simulates the activity of neurons by mathematical model. ANN has obvious advantages in processing fuzzy data, random data and nonlinear data, especially for large-scale, complex structure and uncertain information system. The ANN model was established by employing the dataset in Appendix A.2. This dataset was randomly divided into training set and testing set, 80% and 20% respectively. For the ANN model, the optimal network configuration is (3-20-20-3), in which the number of hidden layers is 2, the number of nodes in each hidden layer is 20, the number of epochs is 1000, and the validation split is 0.2. Rectified Linear Unit (ReLU) was used as the activation function and Sigmoid was utilised as the output transfer function.

3.2.3. Support vector regression

Support vector machine (SVM) is a set of supervised kernel-based machine learning algorithms. It can be employed to classification and regression problems. When the dataset is small, the SVM still has high prediction accuracy. SVM utilises two concepts to obtain an optimal scheme: optimal hyperplane classification and kernel function. The SVR is the SVM conversion for regression analysis. Three conversions of SVM are performed for regression problems: epsilon regression (ε-svr), nu regression (nu-svr), and bound-constraint regression (eps-bsvr). In this paper, ε-svr with radial basis function (RBF) kernel was applied to obtain the SM of the peak folding moment, the peak torsional moment and the torsional failure angle of DCHs. Three hyperparameters need to be tuned to obtain the optimal SVR model, namely the cost of constraint violation (C), epsilon (ε) and gamma (γ). The optimal parameter settings were obtained by using the grid search method, and C = 0.7, ε = 0.001, and γ = 2 were determined.

3.2.4. Random forest

RF is a parallel ensemble learning algorithm for dealing with both regression and classification problems. It utilises multiple decision trees and a bootstrap aggregation technique. If there is a feature missing problem in the dataset, RF can still maintain prediction accuracy and computational efficiency. In addition, it can also resist the overfitting problem and has advantages when handling large dataset with higher dimensionality. RF introduces random attribute selection strategy in the training process of the decision tree. The initial performance of RF is often poor, but with the increase of the number of individual learners, the error of RF will converge to a lower level. Consistent with the ANN model, 80% of the dataset were used as training set and the remaining 20% were utilised as testing set in the RF model. Three hyperparameters must be tuned in the RF model to obtain the optimal results, namely the number of regression trees (n_estimators), maximum depth of regression trees (max_depths) and minimum number of samples required to split internal nodes (min_samples_split). In this study, the best parameters for the RF model are n_estimators = 30, max_depths = 5 and min_samples_split = 10.

3.3. Accuracy evaluation

An indispensable part of benchmarking SMs is evaluating the prediction accuracy to determine the SM with the highest prediction accuracy. Different statistical error functions can be employed to evaluate the performance of SMs, as shown in Table 3. In this paper, RMSE, MAE and R^2 were utilised in regression analysis to compare the prediction accuracy of SMs. RMSE is the average of the square root of the error between the predicted value and the FEA value. MAE is the average absolute error between the predicted value and the FEA value. The smaller the RSME and MAE, the higher prediction accuracy of SMs. R^2 is a value varying between [0, 1], and the closer it is to 1, the smaller the error between the predicted value and the FEA value.

Table 4 shows the values of statistical error functions to compare prediction accuracy of the four SMs. In order to eliminate the influence of randomness of the initial population, the three machine learning models respectively performed 20 predictions and the average values of prediction results were obtained. It is shown in Table 4 that RMSE and MAE of the ANN model are lower than those of the RF model, but higher than those of the RSM model and the SVR model for the peak folding

Table 4
Overall performance metrics of RSM and three machine learning methods.

Models	Peak folding moment			Peak torsional moment			Torsional failure angle		
	RMSE	MAE	R^2	RMSE	MAE	R^2	RMSE	MAE	R^2
RSM	4973	3757	0.971	1289	997	0.991	0.784	0.600	0.943
ANN	7448	5640	0.934	2053	1632	0.976	1.251	0.936	0.855
SVR	4949	3075	0.971	1427	624	0.988	0.858	0.383	0.932
RF	8004	6332	0.924	2770	2074	0.957	1.608	1.177	0.760

Table 5
Parameter definition for four state-of-the-art Genetic Algorithms.

Algorithms	NSGA-III	MOEA/DD	RVEA	SPEA-II
No. of populations	200, 600, 1000, 1500, 2000 and 3000	200, 600, 1000, 1500, 2000 and 3000	200, 600, 1000, 1500, 2000 and 3000	200, 600, 1000, 1500, 2000 and 3000
No. of generations	100	–	100	100
Stop criterion	Reach the max. generation (100)	Reach the total number of fitness evaluation	Reach the max. generation (100)	Reach the max. generation (100)
Crossover rate	0.7	0.7	0.7	0.7
Mutation rate	0.08	0.08	0.8	0.08
Selector operator	Well-spread reference points	Steady-state selection scheme	Angle-based selection criterion	Environmental and mating selection
Elitism operator	Active	Active	Active	Active

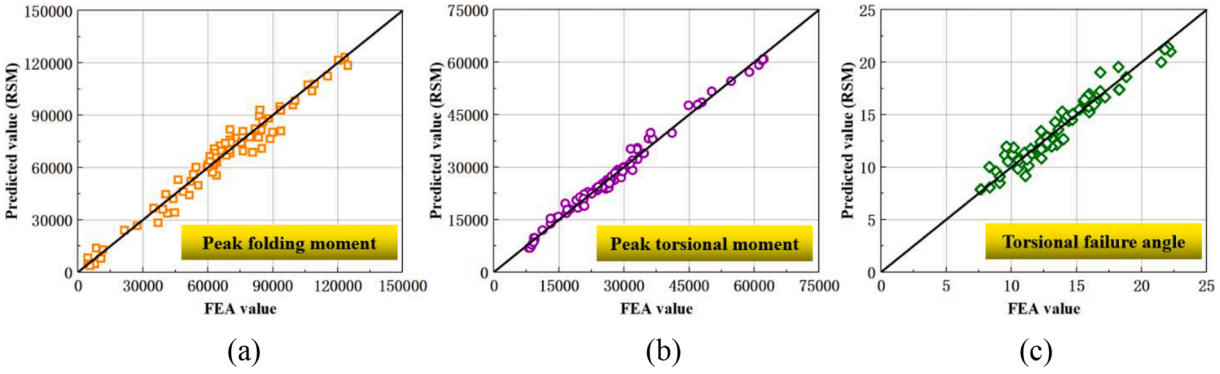

Fig. 8. Scatter plot of the predicted versus FEA values for the RSM model using the Box-Behnken plot: (a) Peak folding moment (b) Peak torsional moment (c) Torsional failure angle.

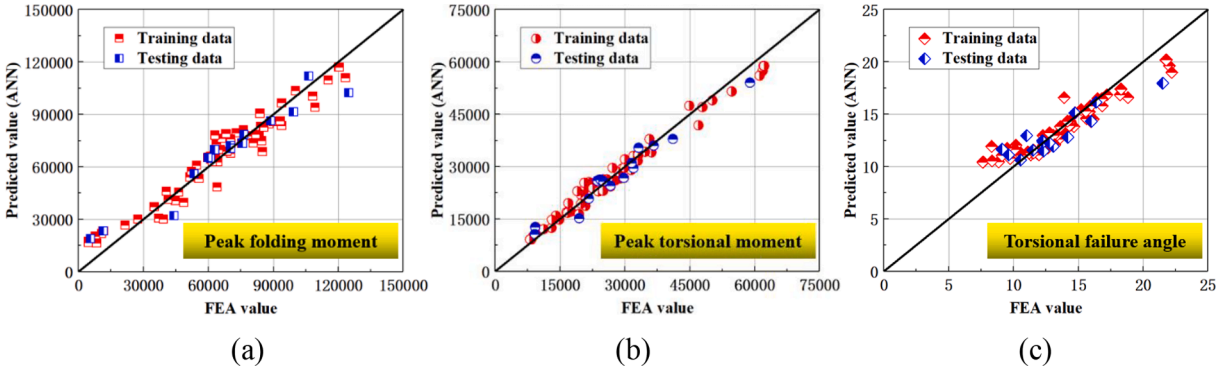

Fig. 9. Scatter plot of the predicted versus FEA values for the ANN model: (a) Peak folding moment (b) Peak torsional moment (c) Torsional failure angle.

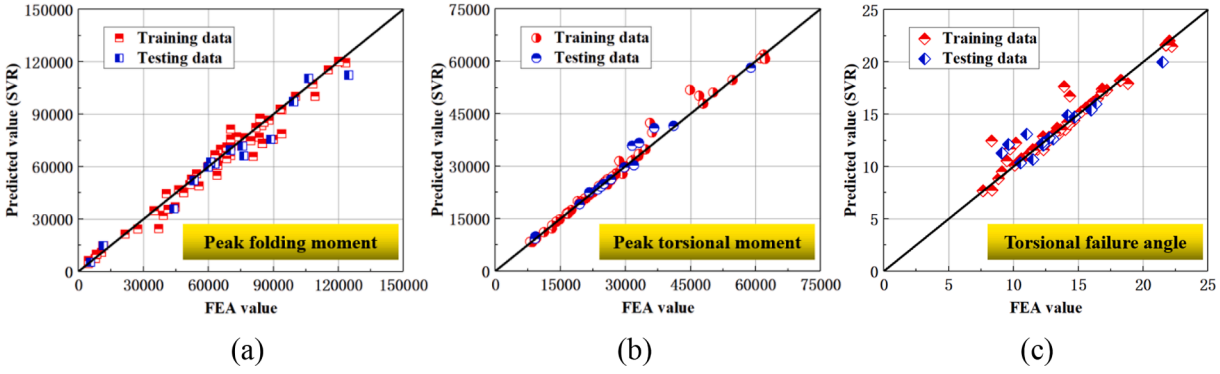

Fig. 10. Scatter plot of the predicted versus FEA values for the SVR model: (a) Peak folding moment (b) Peak torsional moment (c) Torsional failure angle.

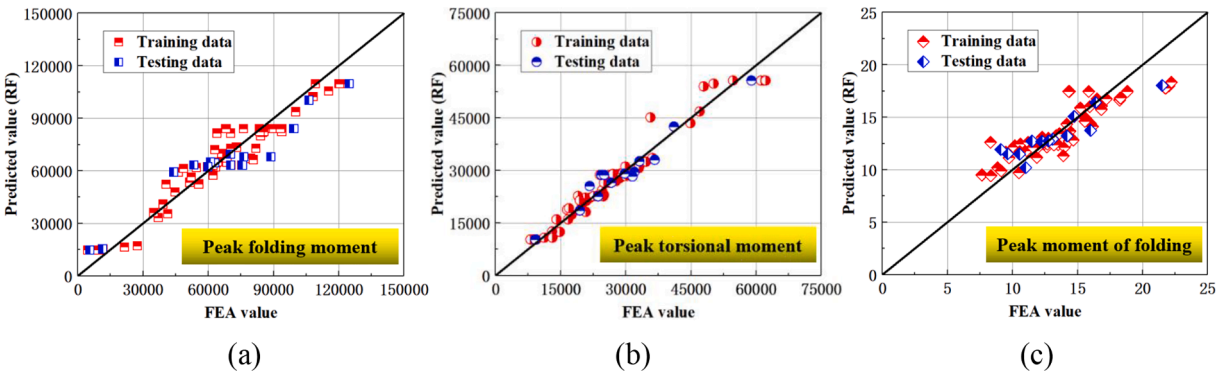

Fig. 11. Scatter plot of the predicted versus FEA values for the RF model: (a) Peak folding moment (b) Peak torsional moment (c) Torsional failure angle.

moment, the peak torsional moment and the torsional failure angle; R^2 of the ANN model is higher than that of the RF model, but lower than that of the RSM model and the SVR model. These results indicate that the RSM model and the SVR model rank the top two, the ANN model is the third place, while the prediction accuracy of the RF model is considered to be the lowest among the four benchmarked SMs. Both the RSM model and the SVR model have very low RMSE and MAE, and high R^2, indicating that both models have high prediction accuracy. It is worth mentioning that there are interesting results when comparing the prediction accuracy of the RSM model and the SVR model. Due to the excellent performance of the RSM model and the SVR model, different results can be obtained through different statistical error functions. For example, for the torsional failure angle, RMSE of the RSM model is lower than that of the SVR model, R^2 is higher than that of the SVR model, but MAE of the RSM model is higher than that of the SVR model. But on the whole, there is little difference between the two models, and both have high prediction accuracy. Hence, it is considered that the RSM model and the SVR model rank first side by side. According to the prediction accuracy, the four benchmarked SMs can be ranked as follows: RSM = SVR > ANN > RF.

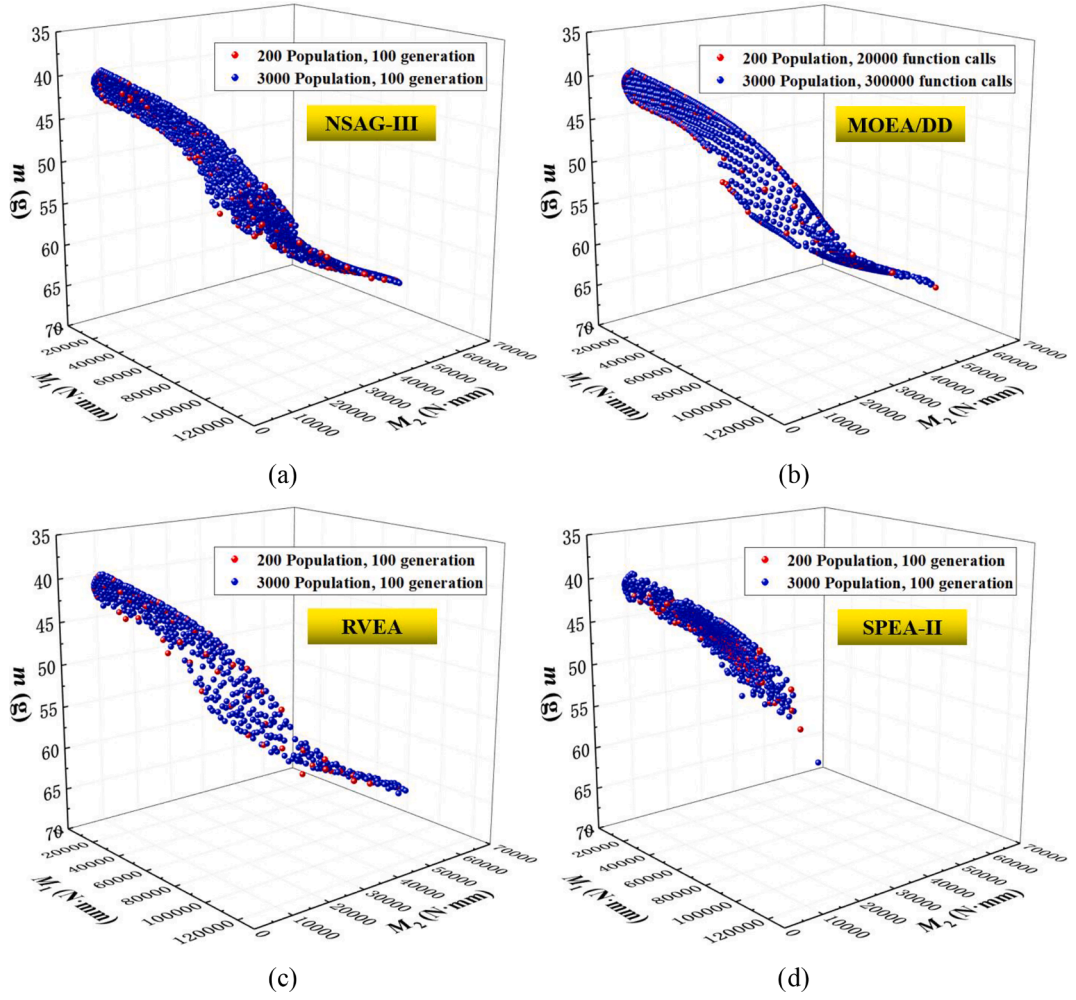

Fig. 12. Comparison of Pareto fronts for different populations sizes: (a) NSGA-III (b) MOEA/DD (c) RVEA (d) SPEA-II.

Figs. 8 to 11 depict the scatter plots of the results of the RSM model and the three machine learning models, in which the results of the three machine learning models include training and testing data. The FEA value is the abscissa (horizontal axis) for each figure whereas the ordinate (vertical axis) represents the predicted value based on the RSM, ANN, SVR and RF models. The black oblique line is the true-prediction line where the predicted value is equal to the FEA value. The points closer to the black oblique line show the better prediction accuracy. It can be easily seen from Figs. 9 to 11 that the RSM model and the SVR model exhibit smaller deviations from the black diagonal than the ANN model and the RF model. Therefore, the prediction accuracy of the RSM model and the SVR model are better than that of the ANN model and the RF model, which is consistent with the conclusion of the above paragraph. In addition, it can be seen from Figs. 9 to 11 that training data and testing data of the three machine models have similar deviations from the black oblique line. There is no overfitting problem, which proves the effectiveness of the three machine learning models.

4. Optimisation of tubular deployable composite hinges

4.1. State-of-the-art Genetic Algorithms

For the multi-objective optimisation problem in this research, three popular hybrid GAs (i.e. NSGA-III, MOEA/DD and RVEA) and a general optimiser SPEA-II were applied to optimise DCHs. Bai et al. [33] introduced the detailed mechanisms and parameters of SPEA-II. The hyperparameters of four state-of-the-art GAs utilised in this optimisation problem are listed in Table 5, in which the selection, crossover and mutation types are default settings. In order to perform a fair test across the four GAs, the same genetic operator types of selection, crossover and mutation were used, as well as the same operator rate which is selected for the CEC'09 benchmarking [34].

4.1.1. Non-dominated sorting genetic algorithm III

NSGA-III is a GA using reference-point-based nondominated sorting method and was first introduced by Deb and Jain [47,48] in 2014. The basic framework of NSGA-III is similar to that of nondominated sorting genetic algorithm II (NSGA-II), but its selection operator and elitism mechanism have changed significantly. The maintenance of diversity among populations in NSGA-III is achieved by providing and adaptively updating many well-spread reference points, rather than through the crowding distance method in NSGA-II. NSGA-III focuses on finding an associated Pareto optimal solution for each reference point. It can identify useless reference points and update reference points adaptively, so the calculation efficiency is higher. For detailed information about NSGA-III, the readers refer to Deb and Jain [47,48].

4.1.2. Multi-objective evolutionary algorithm based on dominance and decomposition

In 2015, Li et al. [49] proposed another leading hybrid multi-objective GA, MOEA/DD, which combines ideas from the decomposition of multi-objective evolutionary algorithm based on decomposition (MOEA/D) with the dominance and niching strategy applied in NSGA-III. MOEA/DD utilises the basic framework of MOEA/D. But in MOEA/DD, the neighborhood is defined based on fixed subregions around each weight vector, whereas in MOEA/D, the neighborhood is defined directly by the nearest Euclidean distances among all the weight vectors. MOEA/DD exhibits excellent performance in the Deb-Thiele-Laumanns-Zitzler (DTLZ) test problem [50]. It also can handle multi-objective optimisation problems with various constraints well. For more detailed information about MOEA/DD, please refer to reference [49].

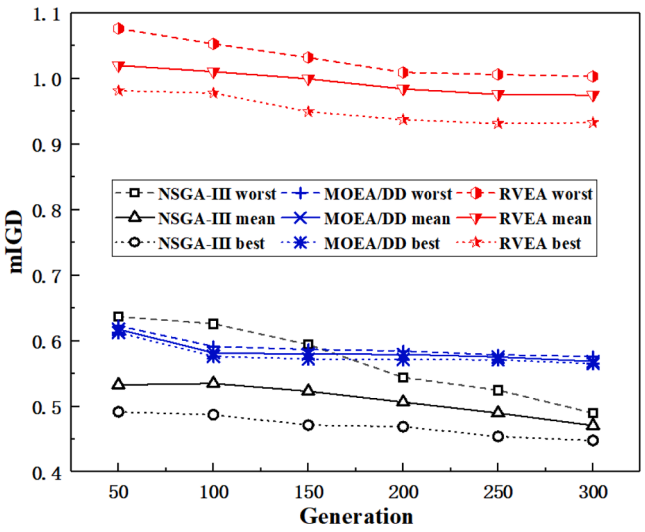

Fig. 13. Comparison of mIGD values for NSGA-III, MOEA/DD and RVEA.

4.1.3 Reference vector guided evolutionary algorithm

In order to solve multi-objective optimisation problems, Cheng et al. [51] presented a reference vector guided evolutionary algorithm (RVEA). RVEA also employs a set of reference vectors to decompose the codomains into many small subspaces. Within each subspace, RVEA inherits an elitism mechanism similar to NSGA-II. The decomposition strategy plays an important role in the performance of hybrid GAs. According to the vector between the reference vector and the candidate solution, the angle penalized distance (APD) is designed to decompose the multi-objective optimisation problems. RVEA calculates fitness values of the candidate solutions by means of APD function. Experimental results show that it exhibits excellent performance in most test sets [50]. A detailed introduction of RVEA is referred to Cheng et al. [51].

4.2. Benchmarking for Genetic Algorithms

Section 3 shows that the RSM model and the SVR model have the best prediction accuracy among the four benchmarked SMs for the peak folding moment, the peak torsional moment and the torsional failure angle of DCHs. It is worth noting that the RSM model has another advantage over other SMs. It is easy to apply and presents an explicit equation of the relationship between design variables and objectives that can be easily tuned under the required conditions. Therefore, based on the RSM model and the analytical formula of mass (i.e. Eqs. (2) and (B-1)-(B-3)), the four popular multi-objective GAs mentioned in Section 4.1 were benchmarked to obtain the optimal designs of DCHs.

In order to obtain the maximum peak torsional moment, the minimum peak folding moment and the minimum mass of DCHs, the influences of population size were studied among the four GAs. According to the review paper from Wang and Sobey [27], the most commonly utilised number of population size is 50 and the most commonly utilised generation numbers are jointly 50 and 100. In order to determine the best population size for each GA, population sizes of 200, 600, 1000, 1500, 2000 and 3000 were compared for the four benchmarked GAs. The runs generating the best Pareto front from 30 simulations are shown

Table 6
League table of the four state-of-the-art Genetic Algorithms.

Genetic Algorithms	Citation frequency	Convergence	Influence of hyperparameters	Computational efficiency	Rank
NSGA-III	2010	Non-convergence	Significant	High	1
MOEA/DD	336	100 Generations	Significant	Medium	2
RVEA	168	200 Generations	Significant	High	3
SPEA-II	7880	–	Significant	Low	4

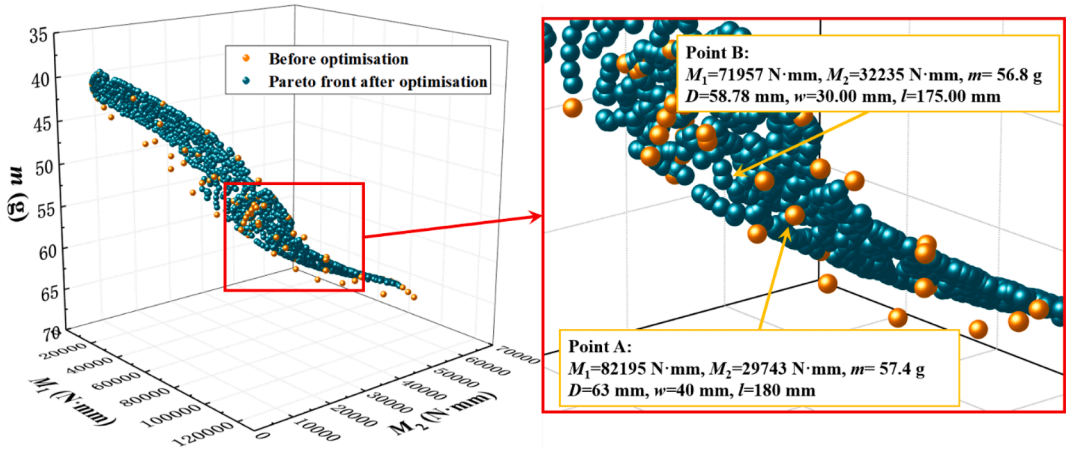

Fig. 14. Optimal designs of tubular DCHs.

in Fig. 12 for the highest and lowest population sizes for each of the four GAs.

The optimisation results of NSGA-III, MOEA/DD and RVEA are similar, all of which are greatly affected by the population size. When the population size is 200, only a few points are on the Pareto front and the design points on the Pareto front is increased with the increase of the population size. When the population size is 3000, NSGA-III, MOEA/DD and RVEA all find similar Pareto fronts. The design points of these GAs are all well distributed, but the density of design points on Pareto front of NSGA-III is larger than that of MOEA/DD and RVEA. SPEA-II is expected to show good performance as a general optimiser, but it has poor performance, as shown in Fig. 12. There is even no design point with the peak torsional moment greater than 35000 N·mm on the Pareto front. SPEA-II is not discussed further due to its poor performance. In the optimisation of tubular DCHs, it is considered that SPEA-II exhibits the worst performance among the four benchmarked GAs.

4.3. Performance metrics

Convergence, distribution diversity and distribution range are three key indicators to quantitatively evaluate the performance of a multi-objective optimiser. Different metrics can be utilised to evaluate the performance of GAs. Commonly used methods of quantitatively evaluating optimisers include: hyper volume (HV) [52], maximum spread (MS) [53], generational distance (GD) [54], inverter generational distance (IGD) [55] and mimicked inverted generational distance (mIGD) [27]. In this study, mIGD was selected as the performance metrics to evaluate the convergence, accuracy and diversity of the Pareto front, and then the best performing optimiser among the four benchmarked GAs was determined. All the Pareto front solutions from all independent run cycles of all the four Gas were combined. Non-domination and duplication checks were implemented on this augmented Pareto front set to filter it and create a 'real Pareto front'. The mIGD values of the obtained Pareto fronts from each GA to this mimicked 'real Pareto front' were calculated to evaluate the performance of each benchmarked GA. The mIGD is determined by using Eq. (15) as [27],

$$mIGD(O, M^*) = \frac{\sum_{\nu \in M} d(\nu, O)}{|M^*|}, \tag{15}$$

where M^* represents a set of points along the mimicked Pareto front, O

Table 7
An optimal design case of a tubular DCH.

Optimal design						
Items	M_1 (N·mm)	M_2 (N·mm)	α(deg)			
FEA value	81,858	29,885	10.56			
RSM model	82,195	29,743	10.64			
Relative deviation	0.41%	−0.48%	0.76%			
Comparison before and after optimisation based on an optimal design						
Items	D (mm)	w (mm)	l (mm)	M_1 (N·mm)	M_2 (N·mm)	m (g)
Before optimisation	63	40	180	82,195	29,743	57.4
After optimisation	58.78	30.00	175.00	71,957	32,235	56.8
Relative deviation	–	–	–	−12.46%	8.38%	−1.05%

represents a set of points from the currently obtained Pareto front, ν is one of the points in the set M^* and $d(\nu, O)$ calculates the minimum Euclidean distance between ν and the points in O. The lower mIGD value reflects the better convergence, accuracy and diversity of the Pareto front.

The mIGD values of the optimisation results obtained by the three better performance optimisers (i.e. NSGA-II, MOEA/DD and RVEA) were recorded from 50 generations to 300 generations with five 50-generation intervals, as shown in Fig. 13. Since all mIGD values of RVEA, including the mean mIGD value among the 30 runs and the mIGD values from the best and worst cases, are higher than those of NSAG-III and MOEA/DD in any generation, illustrating that RVEA has the worst performance of the three GAs. Although all cases from MOEA/DD are better than the worst cases from NSGA-III before 200 generations, the mean mIGD values and the mIGD values from the worst cases of NSGA-III are lower than all mIGD values of MOEA/DD, indicating that the Pareto front of NSGA-III has higher accuracy and diversity. It is clear that NSGA-III has the best performance among the three optimisers. MOEA/DD and RVEA converge at 100 and 200 generations, respectively. NSGA-III has not achieved converged solutions after 300 generations, and the mIGD values gradually decrease with the increased generation number. Therefore, it can be concluded that NSGA-III is expected to perform better when generation is greater than 300. For the optimisation results of MOEA/DD, the difference between the mIGD values of the worst cases and those of the best cases is small, indicating that the Pareto front of MOEA/DD has little difference among the 30 simulations.

In summary, the league table of the four state-of-the-art GAs is shown in Table 6. The four benchmarked GAs are ranked as follows: NSGA-III > MOEA/DD > RVEA > SPEA-II.

5. Design solutions for tubular deployable composite hinges

NSGA-III achieved the best performance among the four optimisers, so the results of NSGA-III with 1500 population size and 200 generations were selected to obtain the optimal designs of DCHs. Due to the repeatability of the results across the four GAs and their 30 independent cycles, it is assumed that each point on the Pareto front is close to the optimal designs of DCHs. There are a total of 1500 design points on the entire Pareto front, and the 1500 design points are sorted in ascending order of mass. Appendix C summarises 16 design points to exhibit how changes in the domain affect the codomains, in which the 16 designs were picked from the first point of each 100 points interval. These 16 design points demonstrate that the relationship between design variables and objectives is nonlinear, which makes design decisions more difficult.

The data satisfying constraints before optimisation is compared with the Pareto front after optimisation, as shown in Fig. 14. It is obvious from Fig. 14 that the data before optimisation is distributed on the lower left side of the Pareto front, which indicates the effectiveness of the optimisation designs. In order to further discuss the optimisation designs, Point A was selected from the data before optimisation and Point B was chosen from the Pareto front by hand. The comparison results of Point A and Point B are shown in Fig. 14 and Table 7. According to Fig. 14 and Table 7, for the DCH ($D = 63$ mm, $w = 40$ mm and $l = 180$ mm), the relative deviations between predicted values of peak folding moment, peak torsional moment and torsional failure angle and FEA values are 0.41%, −0.48% and 0.76% respectively, which further suggests that the RSM model can provide high prediction accuracy. Compared with Point A ($M_1 = 82195$ N·mm, $M_2 = 29743$ N·mm and $m = 57.4$ g), Point B ($M_1 = 71957$ N·mm, $M_2 = 32235$ N·mm and $m = 56.8$ g) is a better design solution. The peak folding moment is reduced by 12.46%, the peak torsional moment is increased by 8.38% and the mass decreased by 1.05%. The results show that a total of 45 design points are found on the Pareto front, all of which are better than Point A for the three objectives (i.e. the minimum peak folding moment, the maximum peak torsional moment and the minimum mass). These 45 design points are listed in Appendix D. Therefore, the coupling RSM-NSGAIII technology is considered to be an effective method to optimise DCHs.

6. Conclusions

Due to lightweight and excellent mechanical properties, DCHs are increasingly used in aerospace field, so it is important to optimise them. In this paper, the coupling SM and GA technology was utilised to obtain the optimal designs of DCHs. The RSM model and three machine learning models were benchmarked, and the SM with the highest prediction accuracy was determined through statistical error functions. In addition, four leading GAs were benchmarked, and the best performing optimiser was determined by applying a performance metric. Three important results emerging from the research are as follows:

The RSM model and three popular machine learning models (i.e. ANN, SVR and RF) were employed as SMs for the peak folding moment, the peak torsional moment and the torsional failure angle of DCHs. The four SMs are sorted according to prediction accuracy by RMSE, MAE and R^2: RSM = SVR > ANN > RF.

The four state-of-the-art multi-objective GAs, namely NSGA-III, MOEA/DD, RVEA and SPEA-II, were benchmarked, and a quantitative analysis metric (mIGD) was applied to determine the best performing optimiser (i.e. NSGA-III). The ranking of the four leading multi-objective GAs is: NSGA-III > MOEA/DD > RVEA > SPEA-II.

Coupling RSM-NSGAIII technology is an effective approach to obtain the optimal designs of DCHs. Compared with Point A, Point B is a better design scheme. The peak folding moment is reduced by 12.46%, the peak torsional moment is increased by 8.38% and the mass decreased by 1.05%. A total of 45 design points are found on the Pareto front, all of which are better than Point A, which helps the designers to efficiently determine their required designs.

CRediT authorship contribution statement

Tian-Wei Liu: Investigation, Validation, Writing – original draft. **Jiang-Bo Bai:** Supervision, Methodology, Writing – review & editing. **Nicholas Fantuzzi:** Supervision, Writing – review & editing. **Guang-Yu Bu:** Software. **Dong Li:** Investigation.

Declaration of Competing Interest

The authors declare that they have no known competing financial interests or personal relationships that could have appeared to influence the work reported in this paper.

Acknowledgements

This project was supported by the National Natural Science Foundation of China (Grant No. 51875026) and the National Defense Basic Research Program of China (Grant No. JCKY2019205C002).

Appendix B. .

$$M_1(D,\ w,\ l) = -7.11 \times 10^6 + 3.95 \times 10^5 D - 36322.2w - 1324.28l + 1284.48Dw - 386.24Dl + 78.42wl - 6541.96D^2 - 222.76w^2 + 55.5l^2 - 0.88Dwl - 6.59D^2w + 6.38D^2l - 2.27Dw^2 - 0.87Dl^2 - 0.58w^2l - 7.569 \times 10^{-3}wl^2 + 31.92D^3 + 2.77w^3 + 6.16 \times 10^{-3}l^3 \quad \text{(B-1)}$$

$$M_2(D,\ w,\ l) = -3.15 \times 10^6 + 1.50 \times 10^5 D + 6305.35w + 1462.54l + 169.58Dw + 132.09Dl - 79.96wl - 2806.71D^2 - 78.07w^2 - 17.61l^2 + 1.18Dwl - 11.16D^2w - 1.4D^2l + 11.09Dw^2 - 0.072Dl^2 - 0.29w^2l + 0.091wl^2 + 20.1D^3 - 4.35w^3 + 0.031l^3 \quad \text{(B-2)}$$

$$\alpha(D,\ w,\ l) = -1038.39 + 45.04D + 8.81w + 0.89l + 0.098Dw + 0.091Dl - 0.069wl - 0.97D^2 - 0.1w^2 - 9.77 \times 10^{-3}l^2 + 7.55 \times 10^{-4}Dwl - 7.79 \times 10^{-3}D^2w - 8.66 \times 10^{-4}D^2l + 8.03 \times 10^{-3}Dw^2 - 7.96 \times 10^{-5}Dl^2 - 7.66 \times 10^{-5}w^2l + 8.61 \times 10^{-5}wl^2 + 8.42 \times 10^{-3}D^3 - 2.95 \times 10^{-3}w^3 + 1.88 \times 10^{-5}l^3 \quad \text{(B-3)}$$

Table A1
Specifications and properties of DCHs [15].

Parameter (unit)	Value
Total length L (mm)	500
Number of the ply	10
Ply angle (deg)	[0/0/45°/−45°/0]s
Thickness of each ply (mm)	0.04
Longitudinal modulus E_1 (GPa)	126
Transverse modulus E_2 (GPa)	8
Poisson's ratio ν_{12}	0.33
In-plane shear modulus G_{12} (GPa)	3.7
Density of composite, ρ (kg/m^3)	1780
Longitudinal tensile strength X_{1t} (MPa)	1050
Transverse tensile strength Y_{1t} (MPa)	40
Longitudinal compressive strength X_{2c} (MPa)	703
Transverse compressive strength Y_{2c} (MPa)	120
In-plane shear strength S_{12} (MPa)	70

Table A2
FEA results for the selected 79 design points [15].

Design No.	D (mm)	w (mm)	l (mm)	M_1 (N·mm)	M_2 (N·mm)	α (deg)
1	65	30	150	68,081	62,023	21.78
2	65	30	160	76,178	61,840	22.02
3	65	30	170	87,935	61,121	22.21
4	65	30	180	99,272	58,887	21.5
5	65	30	190	108,146	54,684	18.82
6	65	30	200	115,272	50,230	15.85
7	65	30	210	120,098	47,927	14.37
8	55	30	150	62,316	20,707	7.67
9	55	30	160	62,510	21,698	8.84
10	55	30	170	62,899	23,593	10.54
11	55	30	180	63,644	24,828	11.86
12	55	30	190	66,170	24,994	12.45
13	55	30	200	72,907	24,994	12.73
14	55	30	210	85,410	24,994	13.08
15	65	50	150	59,822	29,697	12.77
16	65	50	160	59,983	28,865	12.77
17	65	50	170	60,955	27,890	12.72
18	65	50	180	63,287	27,131	12.66
19	65	50	190	70,219	26,063	12.49

(continued on next page)

Table A2 (*continued*)

Design No.	D (mm)	w (mm)	l (mm)	M_1 (N·mm)	M_2 (N·mm)	α (deg)
20	65	50	200	70,218	24,994	12.28
21	65	50	210	70,413	24,182	12.26
22	55	50	150	11,270	9400	14.75
23	55	50	160	10,687	9400	15.22
24	55	50	170	7804	9400	15.93
25	55	50	180	5505	9151	16.37
26	55	50	190	4533	8748	16.49
27	55	50	200	4533	8499	17.20
28	55	50	210	8387	8332	18.28
29	60	40	150	60,955	26,479	11.32
30	60	40	160	60,955	25,823	11.46
31	60	40	170	60,955	26,645	12.30
32	60	40	180	63,287	26,645	12.63
33	60	40	190	70,218	25,563	12.45
34	60	40	200	70,218	25,161	12.68
35	60	40	210	70,218	25,813	13.50
36	55	34	150	54,501	20,524	10.50
37	55	38	150	46,203	20,882	14.00
38	55	42	150	44,002	19,411	15.99
39	55	46	150	36,994	14,832	15.61
40	65	34	150	89,893	46,985	14.35
41	65	38	150	93,769	36,130	10.18
42	65	42	150	83,444	32,991	10.10
43	65	46	150	70,172	31,964	11.49
44	65	34	210	123,258	35,650	8.31
45	65	38	210	124,746	33,148	9.10
46	65	42	210	109,242	31,964	11.09
47	65	46	210	84,002	29,340	12.31
48	55	34	210	84,560	22,550	14.66
49	55	38	210	84,932	19,839	15.99
50	55	42	210	64,021	16,444	16.83
51	55	46	210	39,196	13,049	18.22
52	60	30	180	88,777	31,536	9.62
53	60	34	180	79,410	28,569	9.73
54	60	38	180	65,552	27,728	11.97
55	60	42	180	64,281	24,504	12.81
56	60	46	180	55,599	20,799	13.36
57	60	50	180	44,715	17,543	14.41
58	57	30	150	68,532	25,821	8.34
59	59	30	150	80,636	31,414	9.12
60	61	30	150	76,301	36,624	11.01
61	63	30	150	63,004	44,862	13.90
62	57	30	210	83,750	27,144	11.55
63	59	30	210	93,788	29,980	10.61
64	61	30	210	100,189	34,633	11.20
65	63	30	210	106,241	41,070	13.07
66	57	50	210	21,485	11,226	16.82
67	59	50	210	41,357	14,052	15.56
68	61	50	210	51,452	16,915	14.31
69	63	50	210	62,131	19,002	12.28
70	57	50	150	27,362	13,123	14.17
71	59	50	150	34,910	16,723	13.61
72	61	50	150	40,513	19,846	12.77
73	63	50	150	52,093	23,830	12.42
74	55	40	180	48,631	19,368	16.15
75	57	40	180	53,315	21,647	14.19
76	59	40	180	61,812	24,961	13.19
77	61	40	180	68,592	27,048	11.55
78	63	40	180	81,858	29,885	10.56
79	65	40	180	93,152	33,082	9.50

Appendix C. .

Design No.	D (mm)	w (mm)	l (mm)	M_1 (N·mm)	M_2 (N·mm)	m (g)
1	55.00	50.00	210.00	13,807	6865	39.2
2	55.00	48.03	208.03	23,606	11,640	41.1
3	55.00	47.37	199.48	22,042	13,114	42.3
4	55.00	48.99	171.25	9153	11,436	43.5
5	55.24	44.60	193.34	34,042	17,803	44.9
6	56.04	42.83	201.39	50,014	20,320	46.4
7	56.27	39.29	209.78	70,639	22,216	48.0
8	56.76	40.23	178.77	54,004	22,572	50.1
9	61.66	48.78	168.75	48,044	22,237	52.4
10	58.10	30.00	199.87	83,062	29,482	54.9
11	59.07	30.00	172.98	71,889	32,972	57.3
12	61.19	30.00	181.81	80,293	38,632	59.3
13	62.39	30.00	177.97	82,119	43,580	60.8
14	63.90	30.00	185.56	93,561	49,480	62.2
15	63.68	30.00	150.75	71,867	51,705	63.5
16	65.00	30.60	150.00	75,258	58,463	64.8

Appendix D. .

Design No.	D (mm)	w (mm)	l (mm)	M_1 (N·mm)	M_2 (N·mm)	m (g)
1	57.84	30.00	183.95	73,381	29,951	55.4
2	58.39	30.00	193.13	79,309	30,522	55.6
3	58.06	30.00	183.74	73,758	30,406	55.6
4	58.06	30.13	184.20	74,030	30,190	55.6
5	57.76	30.00	174.76	69,869	29,897	55.7
6	58.68	30.00	194.90	81,003	30,923	55.8
7	58.38	30.00	187.25	76,074	30,882	55.8
8	58.25	30.00	181.63	73,268	30,880	55.9
9	58.39	30.00	183.34	74,284	31,112	56.0
10	58.86	30.00	192.84	80,182	31,469	56.1
11	58.50	30.00	183.88	74,740	31,308	56.1
12	58.16	30.07	175.53	70,959	30,687	56.1
13	58.16	30.07	174.44	70,634	30,686	56.1
14	58.01	30.00	172.69	69,820	30,438	56.1
15	58.66	30.00	187.01	76,568	31,482	56.2
16	59.12	30.00	194.82	81,955	31,804	56.3
17	59.12	30.00	194.82	81,955	31,803	56.3
18	59.05	30.00	194.82	81,808	31,675	56.3
19	58.37	30.18	175.10	71,315	30,984	56.3
20	58.78	30.00	185.29	75,999	31,846	56.4
21	58.81	30.00	182.38	74,754	32,069	56.5
22	58.71	30.00	179.71	73,459	31,950	56.5
23	58.23	30.01	168.91	69,369	30,830	56.5
24	58.83	30.00	180.38	73,963	32,196	56.6
25	58.83	30.00	180.38	73,966	32,196	56.6
26	58.66	30.20	176.06	72,212	31,613	56.6
27	58.65	30.00	174.37	71,516	31,936	56.7
28	59.27	30.07	186.73	77,855	32,727	56.8
29	58.78	30.00	175.00	71,957	32,235	56.8
30	59.28	30.44	183.62	76,660	32,342	56.9
31	58.67	30.20	168.73	70,254	31,585	56.9
32	59.61	30.00	192.42	81,713	33,116	57.0
33	59.61	30.00	193.18	82,163	33,037	57.0
34	59.61	30.00	193.18	82,163	33,037	57.0
35	59.61	30.00	193.18	82,163	33,037	57.0
36	59.61	30.00	193.18	82,165	33,032	57.0
37	58.88	30.00	174.27	71,915	32,478	57.0
38	59.40	30.10	183.15	76,483	33,252	57.1
39	59.01	30.00	172.99	71,784	32,828	57.2
40	58.61	30.00	161.90	68,848	31,393	57.2
41	59.65	30.00	186.50	78,587	33,776	57.3
42	59.07	30.00	172.99	71,889	32,972	57.3
43	58.81	30.00	166.34	69,823	32,189	57.3
44	58.64	30.00	160.35	68,730	31,346	57.3
45	58.64	30.00	160.35	68,730	31,346	57.3

References

[1] Soykasap Ö. Deployment analysis of a self-deployable composite boom. Compos Struct 2009;89(3):374–81.
[2] Sakovsky M, Pellegrino S. Closed cross-section dual-matrix composite hinge for deployable structures. Compos Struct 2019;208:784–95.
[3] Fernandes P, Pinto R, Correia N. Design and optimization of self-deployable damage tolerant composite structures: A review. Composites Part B: Engineering, 2021:109029.
[4] Liu T-W, Bai J-B, Lin Q-H, Cong Q. An analytical model for predicting compressive behaviour of composite helical Structures: considering geometric nonlinearity effect. Compos Struct 2021;255:112908. https://doi.org/10.1016/j.compstruct.2020.112908.
[5] Wang Z, Bai J, Sobey A, Xiong J, Shenoi A. Optimal design of triaxial weave fabric composites under tension. Compos Struct 2018;201:616–24.
[6] Bai JB, Xiong JJ, Gao JP, Yi XS. Analytical solutions for predicting in-plane strain and interlaminar shear stress of ultra-thin-walled lenticular collapsible composite tube in fold deformation. Compos Struct 2013;97:64–75.
[7] Bai J-B, Chen Di, Xiong J-J, Dong C-H. A semi-analytical model for predicting nonlinear tensile behaviour of corrugated flexible composite skin. Compos B Eng 2019;168:312–9.
[8] Bai JB, Chen D, Xiong JJ, Shenoi RA. A corrugated flexible composite skin for morphing applications. Compos B Eng 2017;131:134–43.
[9] Bai J-B, Chen Di, Xiong J-J, Shenoi RA. Folding analysis for thin-walled deployable composite boom. Acta Astronaut 2019;159:622–36.
[10] Bai J, Xiong J. Temperature effect on buckling properties of ultra-thin-walled lenticular collapsible composite tube subjected to axial compression. Chin J Aeronaut 2014;27(5):1312–7.
[11] Mobrem M, Adams DS. Deployment analysis of the lenticular jointed antennas onboard the mars express spacecraft. J Spacecraft Rockets 2009;46(2):394–402.
[12] Fernandes P, Sousa B, Marques R, Tavares JMRS, Marques AT, Jorge RMN, et al. Influence of relaxation on the deployment behaviour of a CFRP composite elastic-hinge. Compos Struct 2021;259:113217. https://doi.org/10.1016/j.compstruct.2020.113217.
[13] Bowen AG, Zucco G, Weaver PM. Morphing of symmetric cross-ply cylindrical shells by minimising the Brazier moment: Optimised hinge folding. Thin-Walled Struct 2021;158:107122. https://doi.org/10.1016/j.tws.2020.107122.
[14] Mallikarachchi HMYC, Pellegrino S. Quasi-static folding and deployment of ultrathin composite tape-spring hinges. J Spacecraft Rockets 2011;48(1):187–98.
[15] Su L, Zhang Y, Sun B. Multi-objective optimization of deployable composite cylindrical thin-walled hinges with progressive damage. Struct Multidiscip Optim 2020;61(2):803–17.
[16] Zhang J, Wang Xu, Liu P, Lei X, Li Z, Gong W, et al. Assessing the weighted multi-objective adaptive surrogate model optimization to derive large-scale reservoir operating rules with sensitivity analysis. J Hydrol 2017;544:613–27.
[17] Ravichandran S, Kumudinidevi RP, Bharathidasan SG, Evangelin Jeba V. Coordinated controller design of grid connected DFIG based wind turbine using response surface methodology and NSGA II. Sustainable Energy Technol Assess 2014;8:120–30.
[18] Ranjbar A, Mahjouri N, Cherubini C. Development of an efficient conjunctive meta-model-based decision-making framework for saltwater intrusion management in coastal aquifers. J Hydro-environ Res 2020;29:45–58.
[19] Hemmat Esfe M, Motallebi SM. Four objective optimization of aluminum nanoparticles/oil, focusing on thermo-physical properties optimization. Powder Technol 2019;356:832–46.
[20] Ding H, Wang Z, Guo Y. Multi-objective optimization of fiber laser cutting based on generalized regression neural network and non-dominated sorting genetic algorithm. Infrared Phys Technol 2020;108:103337. https://doi.org/10.1016/j.infrared.2020.103337.
[21] Hemmat Esfe M, Kiannejad Amiri M, Bahiraei M. Optimizing thermophysical properties of nanofluids using response surface methodology and particle swarm optimization in a non-dominated sorting genetic algorithm. J Taiwan Inst Chem Eng 2019;103:7–19.
[22] Parizad A, Hatziadoniu K. Security/stability-based Pareto optimal solution for distribution networks planning implementing NSGAII/FDMT. Energy 2020;192:116644. https://doi.org/10.1016/j.energy.2019.116644.
[23] Zoraghi N, Shahsavar A, Niaki STA. A hybrid project scheduling and material ordering problem: modeling and solution algorithms. Appl Soft Comput 2017;58:700–13.
[24] Huang X, Shi C, Zhou J, Lu X, Xu G. Performance analysis and design optimization of heat pipe sink with a variable height fin array under natural convection. Appl Therm Eng 2019;159:113939. https://doi.org/10.1016/j.applthermaleng.2019.113939.
[25] Zhang L, Long Z, Cai J, Luo F, Fang J, Wang MY. Multi-objective optimization design of a connection frame in macro–micro motion platform. Appl Soft Comput 2015;32:369–82.
[26] Guo H-N, Wu S-B, Tian Y-J, Zhang J, Liu H-T. Application of machine learning methods for the prediction of organic solid waste treatment and recycling processes: A review. Bioresour Technol 2021;319:124114. https://doi.org/10.1016/j.biortech.2020.124114.
[27] Wang ZhenZhou, Sobey A. A comparative review between Genetic Algorithm use in composite optimisation and the state-of-the-art in evolutionary computation. Compos Struct 2020;233:111739. https://doi.org/10.1016/j.compstruct.2019.111739.
[28] Kaushal A, Alexander R, Rao PT, Prakash J, Dasgupta K. Artificial neural network, Pareto optimization, and Taguchi analysis for the synthesis of single-walled carbon nanotubes. Carbon Trends 2021;2:100016. https://doi.org/10.1016/j.cartre.2020.100016.
[29] Yen GG, He Z. Performance metric ensemble for multiobjective evolutionary algorithms. IEEE Trans Evol Comput 2014;18(1):131–44.
[30] Montemurro M, Vincenti A, Vannucci P. The Automatic Dynamic Penalisation method (ADP) for handling constraints with genetic algorithms. Comput Methods Appl Mech Eng 2013;256:70–87.
[31] Karafotias G, Hoogendoorn M, Eiben AE. Parameter control in evolutionary algorithms: trends and challenges. IEEE Trans Evol Comput 2015;19(2):167–87.
[32] Barbosa HJC, Lemonge ACC, Bernardino HS. A critical review of adaptive penalty techniques in evolutionary computation. Evolutionary Constrained Optimization 2015:1–27.
[33] Bai J-B, Liu T-W, Wang Z-Z, Lin Q-H, Cong Q, Wang Y-F, et al. Determining the best practice – Optimal designs of composite helical structures using Genetic Algorithms. Compos Struct 2021;268:113982. https://doi.org/10.1016/j.compstruct.2021.113982.
[34] Zhang Q, Suganthan PN. Final report on CEC'09 MOEA competition. In: Congress on evolutionary computation (CEC 2009). 2009.
[35] Ferreira SLC, Bruns RE, da Silva EGP, dos Santos WNL, Quintella CM, David JM, et al. Statistical designs and response surface techniques for the optimization of chromatographic systems. J Chromatogr A 2007;1158(1-2):2–14.
[36] Handhal AM, Al-Abadi AM, Chafeet HE, Ismail MJ. Prediction of total organic carbon at Rumaila oil field, Southern Iraq using conventional well logs and machine learning algorithms. Mar Pet Geol 2020;116:104347. https://doi.org/10.1016/j.marpetgeo.2020.104347.
[37] Shozib IA, Ahmad A, Rahaman MSA, Abdul-Rani AM, Alam MA, Beheshti M, et al. Modelling and optimization of microhardness of electroless Ni-P-TiO2 composite coating based on machine learning approaches and RSM. J Mater Res Technol 2021;12:1010–25.
[38] Choi HS, Shin M-S. Hydrodynamics study of two different inverse fluidized reactors for the application of wastewater treatment. Korean J Chem Eng 1999;16(5):670–6.
[39] Malik MH, Arif AFM. ANN prediction model for composite plates against low velocity impact loads using finite element analysis. Compos Struct 2013;101:290–300.
[40] Hussain S, Khan H, Gul S, Steter JR, Motheo AJ. Modeling of photolytic degradation of sulfamethoxazole using Boosted regression tree (BRT), artificial neural network (ANN) and response surface methodology (RSM); Energy consumption and intermediates study. Chemosphere 2021;276:130151. https://doi.org/10.1016/j.chemosphere.2021.130151.
[41] Foroutan R, Mohammadi R, Ramavandi B. Waste glass catalyst for biodiesel production from waste chicken fat: Optimization by RSM and ANNs and toxicity assessment. Fuel 2021;291:120151. https://doi.org/10.1016/j.fuel.2021.120151.
[42] Venkatesh Prabhu M, Karthikeyan R. Comparative studies on modelling and optimization of hydrodynamic parameters on inverse fluidized bed reactor using ANN-GA and RSM. Alexandria Eng J 2018;57(4):3019–32.
[43] Degtyarev VV. Neural networks for predicting shear strength of CFS channels with slotted webs. J Constr Steel Res 2021;177:106443. https://doi.org/10.1016/j.jcsr.2020.106443.
[44] Yang H, Deng Z, Liu R, Wang Y, Guo H. Optimizing the qusai-static folding and deploying of thin-walled tube flexure hinges with double slots. Chin J Mech Eng 2014;27(2):279–86.
[45] Willmott CJ, Ackleson SG, Davis RE, et al. Statistics for the evaluation and comparison of models. J Geophys Res 1986;33(3):250.
[46] Onu CE, Nwabanne JT, Ohale PE, Asadu CO. Comparative analysis of RSM, ANN and ANFIS and the mechanistic modeling in eriochrome black-T dye adsorption using modified clay. S Afr J Chem Eng 2021;36:24–42.
[47] Deb K, Jain H. An evolutionary many-objective optimization algorithm using reference-point-based nondominated sorting approach, Part I: solving problems with box constraints. IEEE Trans Evol Comput 2014;18(4):577–601.
[48] Jain H, Deb K. An evolutionary many-objective optimization algorithm using reference-point-based nondominated sorting approach, Part II: handling constraints and extending to an adaptive approach. IEEE Trans Evol Comput 2014;18(4):602–22.
[49] Li Ke, Deb K, Zhang Q, Kwong S. An evolutionary many-objective optimization algorithm based on dominance and decomposition. IEEE Trans Evol Comput 2015;19(5):694–716.
[50] Liu R, Liu J, Zhou R, Lian C, Bian R. A region division based decomposition approach for evolutionary many-objective optimization. Knowl-Based Syst 2020;194:105518. https://doi.org/10.1016/j.knosys.2020.105518.
[51] Cheng R, Jin Y, Olhofer M, Sendhoff B. A reference vector guided evolutionary algorithm for many-objective optimization. IEEE Trans Evol Comput 2016;20(5):773–91.
[52] While L, Bradstreet L, Barone L. A Fast Way of Calculating Exact Hypervolumes. IEEE Trans Evol Comput 2012;16(1):86–95.
[53] Zitzler E, Deb K, Thiele L. Comparison of multiobjective evolutionary algorithms: empirical results. Evol Comput 2000;8(2):173–95.
[54] Elarbi M, Bechikh S, Said LB. On the importance of isolated infeasible solutions in the many-objective constrained NSGA-III. Knowl-Based Syst 2021;227:104335. https://doi.org/10.1016/j.knosys.2018.05.015.
[55] Cheng S, Zhan H, Shu Z, Fan H, Wang B. Effective optimization on Bump inlet using meta-model multi-objective particle swarm assisted by expected hyper-volume improvement. Aerosp Sci Technol 2019;87:431–47.